Journal of Structural Geology 47 (2013) 3–15

Contents lists available at SciVerse ScienceDirect

Journal of Structural Geology

journal homepage: www.elsevier.com/locate/jsg

Shear-enhanced compaction bands formed at shallow burial conditions; implications for fluid flow (Provence, France)

Gregory Ballas [a,*], Roger Soliva [a], Jean-Pierre Sizun [b], Haakon Fossen [c,d,e], Antonio Benedicto [f], Elin Skurtveit [c,d,g]

[a] U.M.R. C.N.R.S. 5243 Géosciences Montpellier, University of Montpellier II, U.F.R. Sciences et Techniques, Place Eugène Bataillon, 34095 Montpellier cedex 5, France
[b] U.M.R. C.N.R.S. 6249 Chrono-Environnement, Département Géosciences, U.F.R. Sciences et Techniques, University of Franche-Comté, 16 route de Gray, 25030 Besançon cedex, France
[c] Centre for Integrated Petroleum Research (CIPR), Uni Research, Allégaten 41, N-5007 Bergen, Norway
[d] Department of Earth Science, University of Bergen, Allégaten 41, N-5007 Bergen, Norway
[e] Museum of Natural History, University of Bergen, Allégaten 41, Postboks 7800, N-5020 Bergen, Norway
[f] AREVA NC, BU Mines Direction Géosciences, 92084 La Défense, Paris, France
[g] Norwegian Geotechnical Institute (NGI), Sognsveien 72, N-0855 Oslo, Norway

ARTICLE INFO

Article history:
Received 11 June 2012
Received in revised form
19 November 2012
Accepted 21 November 2012
Available online 12 December 2012

Keywords:
Compaction band
Deformation band
Porous sandstone
Permeability
Fluid flow
Shallow burial conditions

ABSTRACT

Field observations of highly porous and permeable sandstone in the Orange area (S-E Basin, France) show that networks of shear-enhanced compaction bands can form in a contractional regime at burial depths of about 400 m ± 100 m. These bands show equal compaction and shear displacements, are organized in conjugate and densely distributed networks, and are restricted to the coarse-grained (mean grain diameter of 0.6 ± 0.1 mm) and less porous (porosity of 26 ± 2%) sand layers. The bands are crush microbreccia with limited grain comminution and high grain microfracture density. They show reductions of permeability (mD) ranging from 0 to little more than 1 order of magnitude. They show no control on the alteration products related to meteoric water flow, which suggests that these shear-enhanced compaction bands have no or only negligible influence on subsurface fluid flow. Their selective occurrence and small (20%) reduction in transmissibility in densely populated layers prevented them from compartmentalizing the sandstone reservoirs. A comparison with compaction-band populations in the Navajo and Aztec sandtsones (western U.S.) emphasizes the role of burial depth and the presence of chemical compaction processes for the sealing potential of deformation bands.

1. Introduction

Deformation bands are tabular strain localization structures found in porous sandstones (Aydin, 1978). These bands are characterized by changes in rock microstructure by grain rearrangement, cataclasis and/or cementation processes, and can form in shear, dilation (mode I), compaction (mode −I), or by combinations of shear and dilation or, more commonly, shear and compaction (see Aydin et al., 2006; or Fossen et al., 2007; for a review). These structures can cause large changes in the petrophysical properties of sandstones and may therefore have an impact on fluid flow in a reservoir setting (Antonellini and Aydin, 1994; Ogilvie and Glover, 2001; Fossen and Bale, 2007; Tueckmantel et al., 2010; Ballas et al., 2012).

Although their formation mechanisms are debated (Schultz and Siddarthaan, 2005; Wibberley et al., 2007), the most common is shear deformation with a shear-perpendicular shortening component (Antonellini et al., 1994; Antonellini and Aydin, 1994, 1995; Saillet and Wibberley, 2010; Tueckmantel et al., 2010), whereas mode I (Dubernard et al., 2002) and mode −I (Mollema and Antonellini, 1996; Sternlof et al., 2005) are less common and therefore poorly described. Eichhubl et al. (2010) recently described shear-enhanced deformation bands, a transitional type of band between shear-dominated and pure compaction bands, from Valley of Fire, Arizona, where they act as a membrane seal for subsurface groundwater flow. The sealing potential of compaction and shear-enhanced compaction bands relative to their conditions of formation, particularly the burial depth and host rock properties, remains to be quantified by petrophysical and mechanical analysis of new field examples.

In this paper, we analyze a network of kinematically consistent shear-enhanced compaction bands formed at shallow burial

* Corresponding author. Tel.: +33 467143643.
E-mail addresses: gregory.ballas@gm.univ-montp2.fr, gregory.ballas@yahoo.fr (G. Ballas).

0191-8141/$ – see front matter © 2012 Elsevier Ltd. All rights reserved.
http://dx.doi.org/10.1016/j.jsg.2012.11.008

conditions during contractional folding of Cretaceous sandstones in Provence, France. We describe the geometry, the microstructure and the petrophysical properties of these bands in regard to their control on alteration products related to subsurface water flow. Hence, we discuss the influence of these bands on fluid flow and their influence on sandstone reservoir properties, and underline the control of burial depth and diagenetic processes on the petrophysical properties of the bands.

2. Geologic setting

2.1. The South-East Basin

The study area is located in the western part of the South-East Basin along both sides of the Rhône Valley, north of the Roquemaure Thrust, France (Fig. 1). Mesozoic rocks in this area contain east-west trending folds that formed during Paleocene to early Oligocene Pyrenean shortening (Sanchis and Seranne, 2000; Lacombe and Jolivet, 2005) between the sinistral strike-slip Cevennes and Nîmes faults (Arthaud and Matte, 1975). This folding is interpreted to be related to thrust ramps cutting partially or entirely through the Mesozoic sedimentary sequence (e.g. Soliva et al., in press). The folds affect limestone and sand-dominated units related to the infilling of the Vocontian basin during the last (Middle to Late Cretaceous) part of the Tethys Ocean sedimentation history (Debrand-Passard et al., 1984). These deposits contain four units of porous and poorly cemented sandstones of Albian, Cenomanian, Turonian, and Santonian ages, respectively (Ferry, 1997) (Fig. 1).

These different sand-dominated units crop out in many places in the western South-East Basin and are actively exploited in numerous sand quarries. The present study is based on samples and field observations from the Boncavaï, Montmout and Tresques sand quarries. The first two quarries are locations of active quartz sand exploitation, and are located on the southern limb of the Mondragon anticline north of the Uchaux normal fault (Fig. 1), while the Tresques quarry is an active sand quarry located on the hinge of the Sabran syncline a few kilometers west of the Bagnols normal fault (Fig. 1).

2.2. The Uchaux Sands

The three quarries studied in this work are located in the Turonian Uchaux Sands. This ~120 m thick sand-dominated unit shows oblique laminae organized into meter to multi-meter thick sand layers that represent deltaic tidal bar to beach deposits. The sands are uncemented, except for minor iron-oxide cementation, as shown by the red-brown color in Fig. 2. This iron oxide cementation is related to the flow of water within the sand reservoir (Saillet, 2009; Ballas et al., 2012). Actual aquifers are located a few meters below the quarries. Hence, the sand layers studied here are located in the vadose (unsaturated) zone.

The quarries exhibit alternating sand layers separated by clay and gravel intervals (see the example of the Montmout quarry in Fig. 2). These sand layers show large variations in grain size and porosity, while differences in grain angularity, sorting and clay component are small (see Table 1 for the host sand characteristics). Three different types of sand are identified: (1) well laminated coarse-grained and clean sands, showing a porosity less than 30%; (2) fine-grained and clean sands with porosity values greater than 30%; (3) clay-rich (about 15% of clay) and fine-grained sands, showing a porosity of about 33%.

3. Field data

Two different types of deformation bands were observed at the three sites: (1) normal-sense shear bands (with some compaction), and (2) a large number of bands showing no observable shear offset in outcrop (Saillet, 2009). These two types of bands show different geometrical characteristics, in particular in terms of distribution, thickness, length, and shear/compaction ratio (Soliva et al., in press). This study focuses on the analysis of the second type of bands, for which we measured orientation, dip, length, and shear displacement at each study site (see Ballas et al., 2012; for a detailed

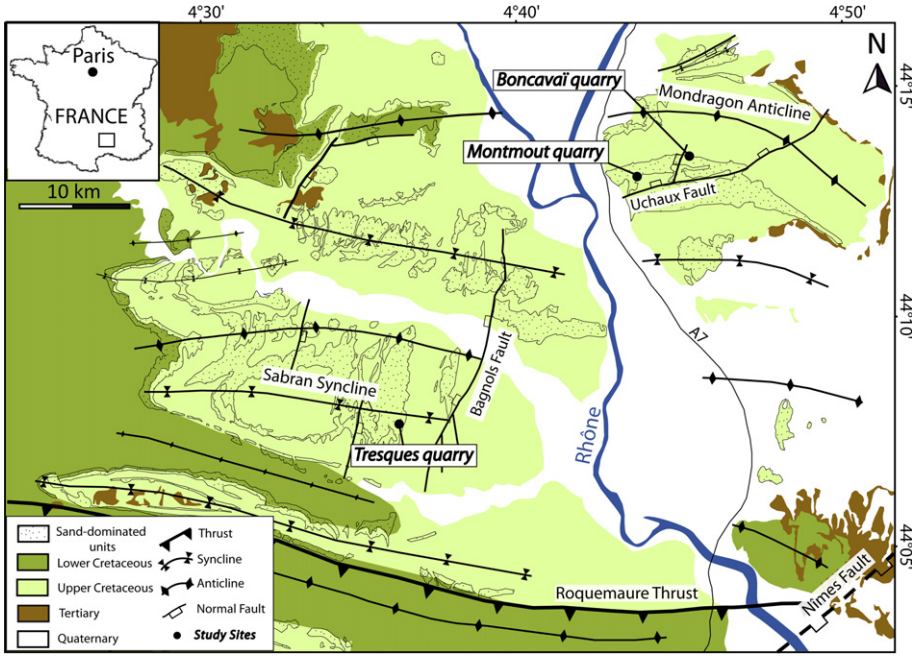

Fig. 1. Geological map of the western part of the South-East Basin, France.

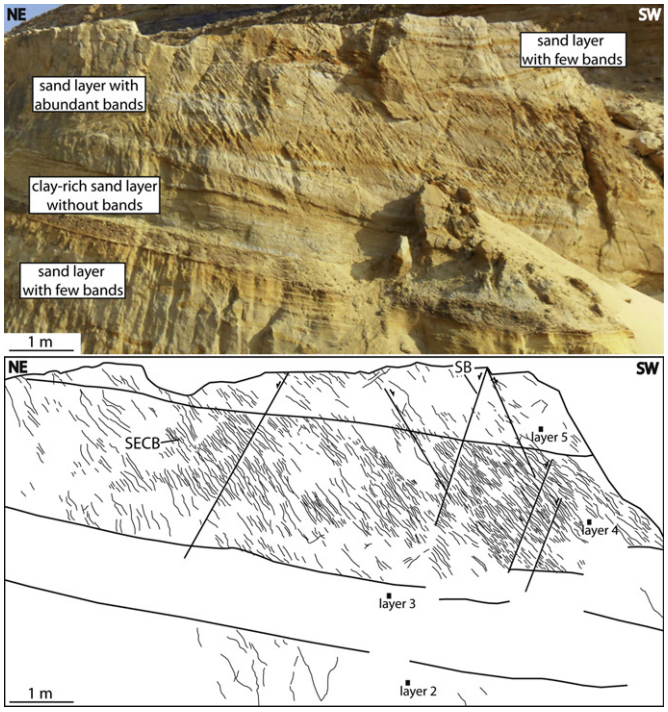

Fig. 2. The alternation of sand layers within the Turonian sand-dominated unit at the Montmout quarry. The SECBs are confined to certain sand layers. The black squares are the locations of the samples used in the microstructual and petrophysical analysis of the host sand.

study of the normal-sense shear bands). Band thickness and spacing were measured along scan-lines oriented perpendicular to the bands in zones of uniformly dipping bands.

3.1. Organization and distribution

The deformation bands are organized into densely distributed and conjugate networks striking N°85E to N°130E (Fig. 3a and b, and Fig. 4), and dipping 30° to the north and 70° to the south in the Boncavaï and Montmout quarries. In the Tresques quarry the two conjugate sets dip 50° to the north and south (Fig. 4). These conjugate sets show a dihedral angle close to 90° (see Table 2 for details) and no systematic cross-cutting relations were observed (Fig. 3b). Actually, intersections between the conjugate sets (Fig. 3c) are rare; typically only one dipping set is developed in any given part of an outcrop (Fig. 2). The number of bands per meter ranges between 30 and 35 in the most densely populated sand layers (5 b/m on average in the other sand layers) (Table 2). These sand layers show a fairly constant band density along the entire outcrop, except for some local zones with few or no bands, in particular in the Boncavaï quarry. The band spacing in these densely populated sand layers is 2.5 cm on average (Table 2), and 87% of the band spacing values fall between 0.5 cm and 5 cm (Fig. 5a). Band spacing greater than 10 cm were measured a few places, preserving local zones of nearly undeformed host rock within overall intensely deformed parts of these sand layers (Fig. 3a). No clear relationship was observed between sand layer thickness and band distribution.

The shear-enhanced compaction bands (SECBs) are preferentially located in specific sand layers within the sand-dominated unit, for example layer 4 in the Montmout quarry (Fig. 2). Unlike the normal sense shear-bands, which may cut an entire sand unit (Fig. 2), most SECBs stop at the boundaries between sand layers, in particular where gravel or clay is abundant in the adjacent layer (Fig. 3d). Greater densities of SECBs are observed in the coarse-grained and less porous sand layers whereas only a few bands are observed in the fine-grained and more porous sand layers (Fig. 2). Furthermore, the few bands that occur in fine-grained sand layers are often physically linked to bands in more deformed layers. For example, we observed that the few bands present in the fine-grained sand layer from the Boncavaï quarry can be traced continuously into the adjacent deformation band-rich sand layer (Fig. 3a and d). No SECBs are observed in the clay-rich sands (Fig. 2).

Table 1
Petrophysical description of the different sand layers investigated in this study.

Layer	Porosity[a] (%)	Median grain diameter[b] (mm)	Composition[c]
Montmout			
Layer 1	21.9	0.55	Quartz: 93.5%, feldspar: 2%, clay: 4.5%
Layer 2	35	0.31	Quartz: 92%, feldspar: 2%, clay: 6%
Layer 3	33	0.21	Quartz: 81.5%, feldspar: 3.5%, clay: 15%
Layer 4	26.7	0.62	Quartz: 93.5%, feldspar: 2%, clay: 4.5%
Layer 5	34.3	0.27	Quartz: 92%, feldspar: 2%, clay: 6%
Boncavai			
Coarse	27.3	0.64	Quartz: 95%, feldspar: 4.5%, clay: 0.5%
Fine	38.8	0.23	Quartz: 96.5%, feldspar: 3%, clay: 0.5%
Tresques	23.4	0.72	Quartz: 94.5%, clay: 5.5%

[a] Porosity was measured by Mercury Injection Porosimetry (MIP).
[b] Mean grain diameter was obtained by laser granulometer and completed by sieving method.
[c] Sand composition was estimated by image analysis from SEM photomicrographs.

3.2. Band characteristics

Each band is observed as a single strand of deformed sand. The band characteristics are quite similar between the three quarries. Band thickness ranges from 0.1 cm to 3.6 cm and the cumulative thickness distribution curves show that 95% of the bands have thickness less than 2 cm (Fig. 5b). The mean thickness is close to 0.5 cm (see Table 2) and no large variation in thickness is observed along the bands. The length of the bands cannot be measured precisely because of the patchy distribution of exposures and the small outcrop size. With respect to global displacement – length relationship for deformation band systems (Schultz et al., 2008), we expect that the length of an isolated band would be several meters. However, these bands have numerous relay zones and eye structures formed during band interaction during growth (Fig. 3a). Such linked networks have a horizontal extent observed to exceed 35 m in the Boncavaï quarry. In contrast, the vertical extent of the bands cannot exceed 10 m because of the limited thickness of deformation band-bearing sand layers.

The deformation bands do not appear to offset the sedimentary lamination, which is obliquely cut by the bands (Fig. 3e). However, there is a component of band-perpendicular compaction ranging from 0.04 to 1.7 mm across individual bands that was estimated by the method described by Soliva et al. (in press) (Table 2). This compaction should induce an apparent normal shear offset of the lamination, which is never observed (Fig. 3e). Hence, the displacement effect of the compaction is assumed to be more or less canceled out by a band-parallel shear displacement of comparable magnitude. Together with the fact that the angle between bedding and the bands is relatively close to 45° (Fig. 4), this interpretation implies that the compaction and shear

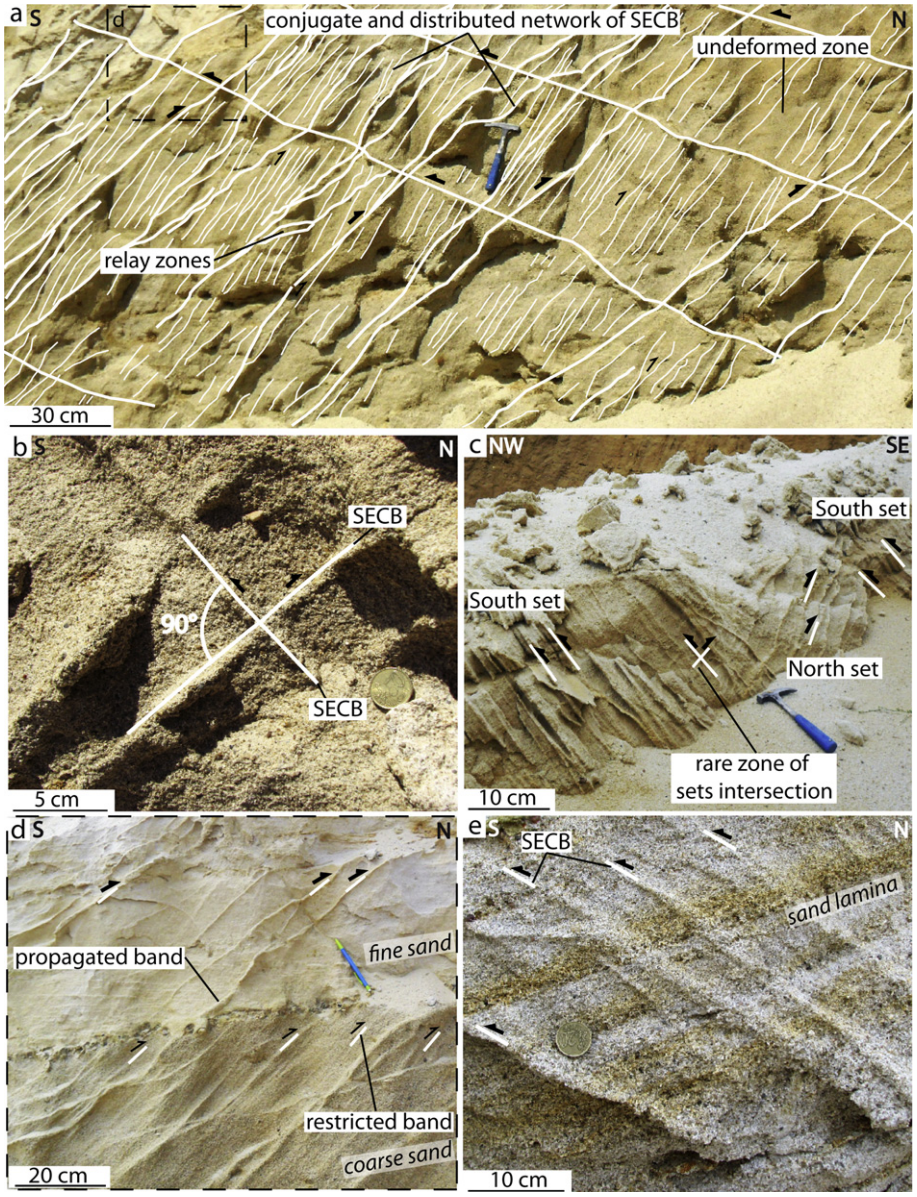

Fig. 3. a. Shear-enhanced compaction bands organized into distributed and conjugate network (Boncavaï quarry). b. The two dipping sets show a dihedral angle close to 90° (Boncavaï quarry). No consistent crosscutting relationships are observed between the two dipping sets. c. Example of rare region where the two sets coexist (Tresques quarry). d. Detailed view of the transition from coarse- to fine-grained sand (Boncavaï quarry). The few SECBs observed in the fine-grained sand are linked to bands in the highly deformed layers. e. The SECBs show no observable shear offsets of the sedimentary lamination.

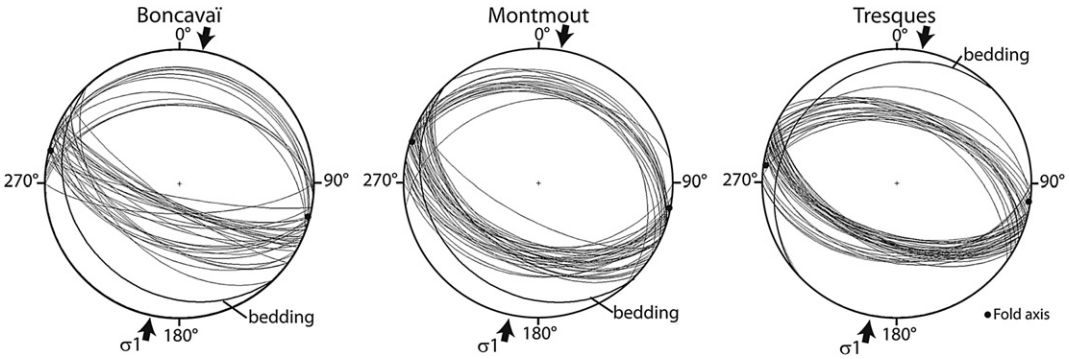

Fig. 4. Orientation of the SECBs, bedding planes, and fold axis for the Boncavaï, Montmout, and Tresques quarries (lower hemisphere projection).

Table 2
Geometric data of the studied bands at each quarry. These characteristics were measured in the sand layers showing the greatest density of bands.

Quarry	Dihedral angle (°)	Band density (b/m)	Average spacing[a] (mm)	Average thickness[b] (mm)	Average compaction[a] (mm)
Montmout	80	34	24	4.4	0.26
Boncavaï	86	31	26	6.8	0.32
Tresques	96	31	25	6.9	0.28

[a] 133, 95, and 156 thickness and compaction were measured in the Montmout, Boncavaï and Treques quarries, respectively.
[b] 132, 96, and 154 band spacing were measured in the Montmout, Boncavaï and Treques, respectively.

components produced similar amounts of displacements, generally at the sub-millimeter scale. Following this line of evidence, the shear-displacement along these bands also ranges between 0.04 and 1.7 mm.

It should be noted that displacements at the submillimeter scale are hard to accurately quantify in these sands, so the shear strain estimate is considered an approximation. Regardless, this finding implies that the amount of shear-displacement increases with the band thickness, and an average ratio of shear-offset/thickness for the bands in the quarries can be estimated at ≈1/20. Any additional strike-slip offset would be difficult to detect, but given the orientations of the conjugate sets of bands and their implications for the orientation of principal stress axes (Fig. 4), strike-slip offset is considered to be unlikely.

3.3. Relationship with the alterations

Alteration products (iron oxides and hydroxides) related to post-Oligocene (i.e. post band formation) meteoric water flow (Ballas et al., 2012) are found to selectively colorize the sands in the quarries. These mineral deposits formed at different depths corresponding to specific flow conditions: red laminations are related to downward flow of water under vadose conditions (Fig. 6a), orange volumes formed during later stages of ground-water drainage subject to water level variations (Fig. 6b), and Liesegang bands are associated with diffusive mass transfer under phreatic conditions (Fig. 6c) (Potter and Chan, 2011). The patterns associated with such mineral deposits with respect to deformation bands have been used in several studies to discuss the membrane seal potential of the bands for water flow (e.g. Taylor and Pollard, 2000; Eichhubl et al., 2004; Parry et al., 2004).

In the quarries in the South-East Basin we see little or no control of SECBs on the distribution of the alteration products. Rather, all cementation patterns pass through the bands without deflection or offset (Fig. 6a–c). Moreover, the bands are internally bleached or colored in a same way as the host rock. In contrast, normal-sense shear bands in the study area generally limit the alteration, as shown in Fig. 6b (also see Ballas et al., 2012).

4. Microstructures

4.1. Methods

18 polished thin-sections from blocks of the host rock and band samples impregnated by epoxy resin were examined by back-scattered electron imagery using a FEI Quanta 200 environmental scanning-electron microscope (SEM). Mosaics of SEM back-scattered electron images, with a gray-scale intensity range from 0 to 255, were obtained and used to calculate the *image analysis porosity* of the bands and the host rocks. The *relative amount of fractured grains* (%) and the *microfracture density* (f/mm^2) were calculated using a square of 1 × 1 mm drawn on mosaics of SEM microphotographs. These textural characteristics are used to quantify and compare the grain-scale structures within and outside of the bands.

The grain-size distributions of host rock and deformation band samples from the different study sites and from different sand layers of the Montmout quarry (Fig. 2) have been measured using a Coulter LS 13 320 laser granulometer and complemented by sieving for the coarse grains (>1 mm in diameter). The grain size distribution has been used to discuss grain comminution and the intensity of cataclastic deformation within the bands.

Mapping of force chains and grain microfractures were performed on photographs of thin sections oriented perpendicular to the band. The force chains are observed as trains of aligned grains that are in contact, and these chains are considered to represent load-bearing structures within the granular framework (Eichhubl et al., 2010; Soliva et al., in press). These structures formed approximately parallel to σ_1 and will be used below to constrain the orientation of stresses and the timing of band formation.

4.2. Textural characteristics

The shear-enhanced compaction bands are millimeter- to centimeter-thick zones that show an increase in grain fracture as compared to the host sand (Fig. 7). Grain fracture is primarily observed at grain contacts and especially in feldspar grains (white

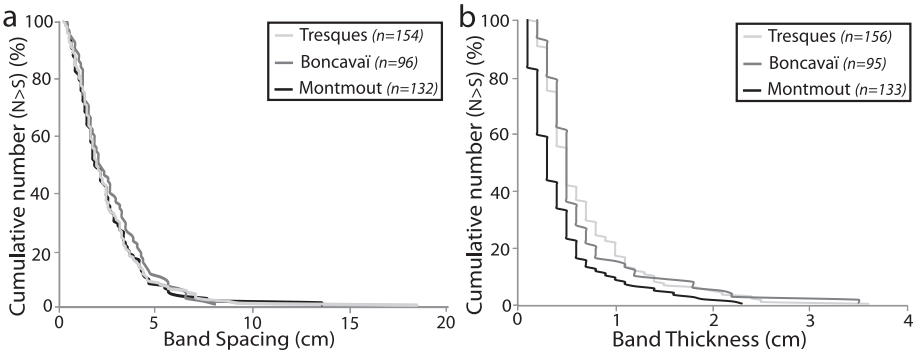

Fig. 5. a. Distribution of the *band spacing*. b. Distribution of the *band thickness*. (***n*** is the number of counts). These parameters have been measured in the sand layers showing the greatest density of SECBs.

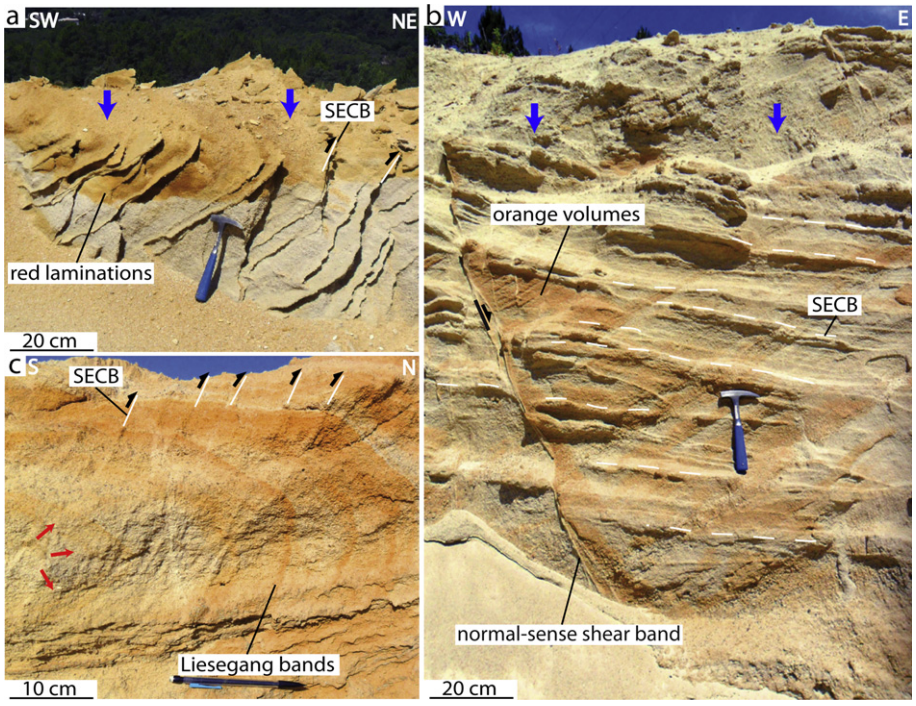

Fig. 6. Relationship between the SECBs and the alteration products associated with post-band meteoric water flow. a. Red lamination formed under vadose conditions. b. Orange volumes induced by ground-water storage. c. Liesegang bands formed under phreatic conditions. Blue and red arrows show the water and the diffusive flow directions, respectively. (For interpretation of the references to colour in this figure legend, the reader is referred to the web version of this article.)

grains in SEM photomicrographs, Fig. 7). No compaction and only slight grain comminution are observed, which make it difficult to identify these bands under the microscope. These bands show quite diffuse borders with the surrounding sand, which also contain some fractured grains (Fig. 7a and c). No significant variation in textural characteristics was observed with respect to band thickness and dip in the Boncavaï quarry (see Fig. 7b and c to compare two thin and thick bands). Similarly, no differences in textural characteristics were observed between the bands from the different sites (see Fig. 7a and c to compare bands with similar thickness but sampled in different quarries).

Even though the amount of fractured grains is high (75%) in the host rock, it is clearly higher in the bands (85–90%) (Fig. 8a). Similarly, the microfracture density is greater within the bands than in the host rock by about 4 fractures/mm^2, showing an increase from ca. 6 fractures/mm^2 in the host rock to 8.6–13.8 fractures/mm^2 in the band (Fig. 8a). The amount of fractured grains and the microfracture density are similar for thin and thick bands (Fig. 7b and c).

SECBs show a somewhat lower porosity than the surrounding host rock. This porosity reduction is consistently reduced from 28% in the host rock to 24% in the band for all the quarries (Fig. 8b). Some large-sized (millimeter-size) pores observed in the host rock microstructure are located within the bands. Rare examples of more strongly deformed SECBs, showing band porosity around 20%, are observed (right-hand outlayer in Fig. 8b).

The grain size distribution curves obtained from the bands are close to that obtained from the host rock (Fig. 9). The bands and the host rocks are composed of large grains with diameter ranging between 0.2 and 1.5 mm. A small increase in the amount of grains with size ranging between 0.2 mm and 0.5 mm and a similarly small reduction in the amount of the largest grain fraction (diameter close to 1 mm) are observed in the bands. This grain-size reduction is therefore revealed by a decrease in the median grain size (Fig. 9b–d). On average, this reduction ranges from 0.524 mm in the host rock to 0.456 mm in the band. This modest grain-size reduction is consistent with the finding that the bands contain less than 10% cataclastic material (particles having diameters $< 10\%$ of the modal grain diameter of the host sand) (Figs. 7 and 9). Following the terminology proposed by Sibson (1977), these SECBs are classified as crush microbreccia (e.g. Scholz, 1990).

The force chains around the SECBs are oblique to the band (see Fig. 7 and Fig. 10a). These force chains statistically make an angle of 30°–50° to the band, with an average angle (α_m) about 45° (Fig. 11a). Each force chains consists on average of 3–4 grains (Fig. 10a), and their length ranges from 0.3 to 4 mm with an average of 1.3 mm. These results are similar for bands from the different quarries. Microfractures are developed at grain contacts consistent with Hertzian contacts (Fig. 7d and Fig. 10b). These grain microfractures are oriented subparallel to the force chains, ranging from 30° to 50° to the band (Fig. 11b). A difference in microfracture orientation by a few percent is sometimes observed between grains in the bands and grains outside the bands, with the average microfracture angle within the bands being slightly greater (up to 50° to the band). The orientations of grain microfractures in the host rock sampled far from the bands are similar to the microfracture orientations measured close to the bands.

5. Petrophysical properties

5.1. Methods

Porosity, *specific surface area* and distribution of *pore access radius*, which ranges from 0.003 to 215 μm, were obtained by Mercury Injection Porosimetry (MIP) using a Micromeritics Pore-Sizer Autopore IV porosimeter. The *median pore access radius* (R_{50}) corresponding to the pore access radius for which 50% of the pore volume is reached by the mercury, was used and plotted against

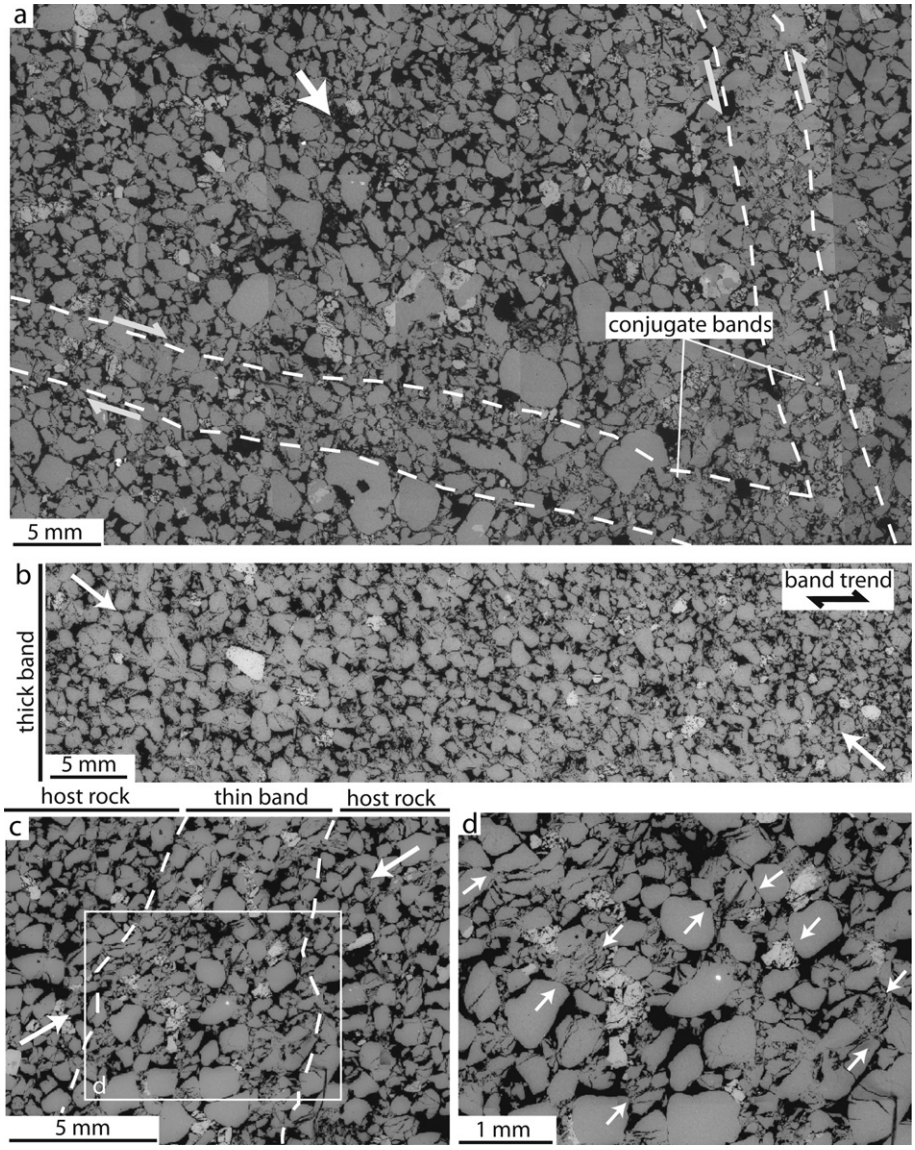

Fig. 7. a. Photomicrographs of the conjugate SECBs from the Montmout Quarry. b. Photomicrograph of the internal structure of a thick SECB from the Boncavaï quarry. c. and d. Detailed view and close-up of the microstructure of a thin SECB from the Boncavaï Quarry. White arrows show the direction of σ_1 at the time of band formation. Dashed lines are band boundaries.

porosity (Fig. 12a) to quantify the porous network changes within the deformation bands. 29 measurements were made on host rock and band samples for the three different sites. *Permeability* (k) was estimated using the Kozeny–Carman law (1) described in Torabi et al. (2008) for image analysis.

$$k = \phi^2/cFs^2 \tag{1}$$

where ϕ the porosity, c is a constant related to pore geometry that equals 2 for pores having a circular cross-section, F is the formation factor ($F = \phi^{-m}$ where $m = 1.5$ for uncemented rocks) and s is the specific surface area calculated from MIP data, assuming a cylindrical pore model. These calculated permeability values were calibrated by gas permeability measurements on cores of normal-sense shear bands (see Ballas et al., 2012, for permeability calibration).

Transmissibility multiplier (T) of the deformed sand layers was calculated from equation (2) of Manzocchi et al. (1999) for fluid-flow simulation models. The reservoir transmissibility multiplier equals 1 for undeformed sand layers and approximates 0 with the presence of impermeable structure. This transmissibility multiplier is expressed as:

$$T = \left[1 + \left(t_f/L\right)\left(\left(k_m - k_f\right)/k_f\right)\right]^{-1} \tag{2}$$

where t_f/L is the band thickness/layer thickness ratio, k_m is the host rock permeability, and k_f the average band permeability. A t_f/L ratio of 0.2 was used for the highly deformed sand layers.

5.2. Porosity and porous network

Shear-enhanced compaction bands are zones of reduced porosity in the sands. This reduction in porosity is very similar for the different sites, i.e. from 28% in the host rock to 24% in the bands of the Boncavaï quarry, from 27% in the host rock to 24% in the bands of the Montmout quarry, and from 24% in the host rock to 21% in the bands of the Tresques quarry (Fig. 12a). Porosity was

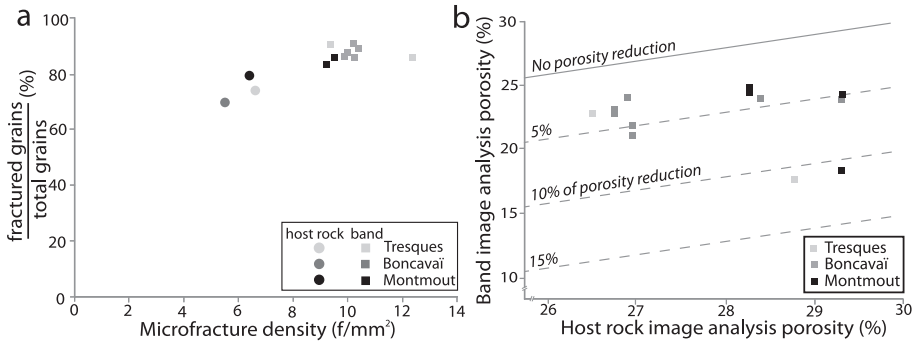

Fig. 8. a. Plot of the fractured grains ratio vs. the microfracture density. b. Plot of the band image analysis porosity vs. host rock image analysis porosity.

also measured in bands in more porous and fine-grained sand layers at the Montmout quarry, and these bands show a porosity reduction from 35% in the host rock to 27% in the bands. This porosity reduction is greater than the porosity reduction in the bands of the less porous and coarse-grained sands. All together, these porosity reductions are less than 8%. We also observe a close correlation between mercury porosity and image analysis porosity (see Section 4.2).

Mercury injection data show a pore network within the bands that is composed of smaller access radii than in the host rock. The distribution curves for pore access radius (not shown here) reveal a pore access decrease within the bands. This reduction is confirmed by a decrease of the median pore access radius from 44 μm in the host rock to 33 μm in the bands of the Boncavaï quarry, and from 45 μm in the host rock to 27 μm in the bands of the Montmout and Tresques quarries (Fig. 12a). The reduction of the median pore access radius (R_{50}) remains limited, i.e. 36 μm of R_{50} reduction in the higher-strain bands from the Tresques quarry. The porous network of SECBs is therefore typified by large pore throats.

5.3. Permeability and transmissibility

The shear-enhanced compaction bands studied here show lower permeability values than the host sands. We observed a permeability reduction ranging from 0 to 1.2 orders of magnitude from host rocks to bands (Fig. 12b). For the Boncavaï quarry, permeability was estimated across bands with different dips and thicknesses, showing a reduction in permeability of about 0.5 order of magnitude for each measured band, i.e. the host rock permeability is about 1770 mD, and the band permeability ranges from 652 mD to 1596 mD. This result shows that band thickness and dip have no control on permeability. In the Montmout and Tresques quarries, some bands show permeability reduction in excess of 1 order of magnitude (Fig. 12b). A close investigation of these bands show that these cases of greater permeability reduction are associated with more intense microfracture, a higher level of grain communition and a higher porosity reduction. Altogether, however, the reduction in permeability in the deformation bands is relatively small, rendering the shear-enhanced compaction bands as highly permeable structures.

The presence of the SECBs reduces the reservoir transmissibility. The transmissibility multipliers calculated for the highly deformed sand layers of the Boncavaï, Moutmout and Tresques quarries are about 0.92, 0.61, and 0.81, respectively. However, the transmissibility reduction calculated for the coarse-grained sand layers of the Montmout quarry (0.61) seems overestimated because it is based on only one band permeability estimate and shows one of the greatest permeability reductions for this study at about 1 order of

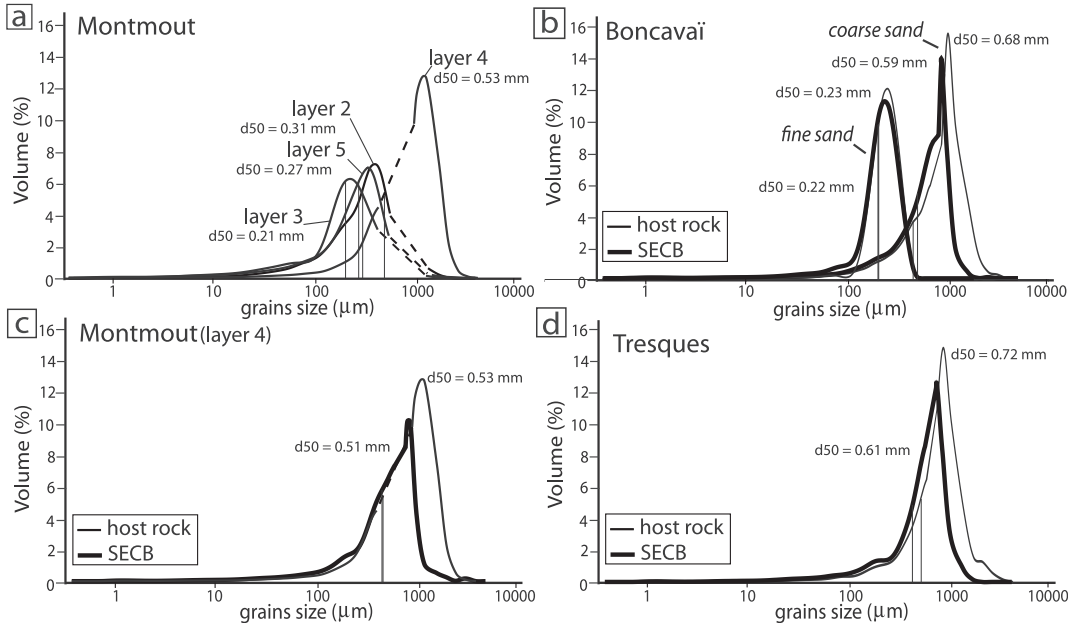

Fig. 9. a. Grain-size distributions of the different sand layers at Montmout quarry. b. c. and d. Grain-size distributions of the host rock and bands at the Boncavaï, Montmout and Tresques quarries.

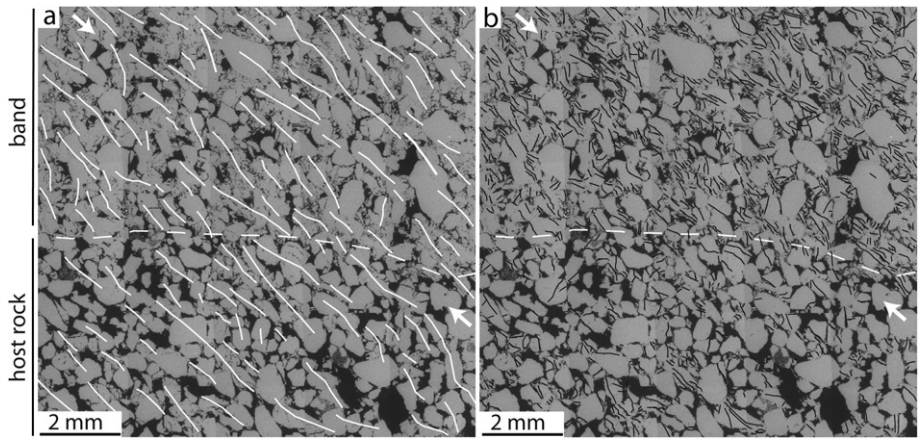

Fig. 10. Maps of force chains (a) and grain microfractures (b) on SEM photomicrograph of a SECB from a coarse-grained sand at the Tresques Quarry.

magnitude, which is probably not representative for all bands of this quarry. The transmissibility reduction induced by the presence of the SECBs in the more strongly deformed sand layers ranges between 10% and 20%. The transmissibility of the fine-grained sand cannot be calculated because of the variability of the band distribution in these layers.

6. Discussion

6.1. Timing and shallow burial conditions

The orientation of bands and folds are consistent with the regional Pyrenean stress field (Fig. 4), which from various contractional structures is determined to have a horizontal and N-S oriented σ_1 axis and a vertical σ_3 axis. In this stress field, the shear-enhanced compaction bands can be interpreted as Andersonian conjugate systems with σ_1 axis oriented parallel to the bedding and normal to the line of band intersection, and showing force chains oblique to the bands by an angle of 37–55° (Olsson, 2000; David et al., 2001; Eichhubl et al., 2010). In the Tresques quarry, located in the hinge of the Sabran Syncline, the band organization (Fig. 3a, d and Fig. 4) and the orientation of the force chains (Fig. 10) are consistent with a horizontal σ_1. In contrast, in the Boncavaï and Montmout quarries bedding dips 20° S, the bands dip about 70° S and 30° N, and the force chains dip 20° (Figs. 10 and 11). These relations are consistent with a horizontal σ_1 at the time of band formation, which happened before or at the initial stages of folding (Fig. 13a and b), and a 20° southward tilting of bands and bedding related to the Mondragon anticline development (Fig. 13c).

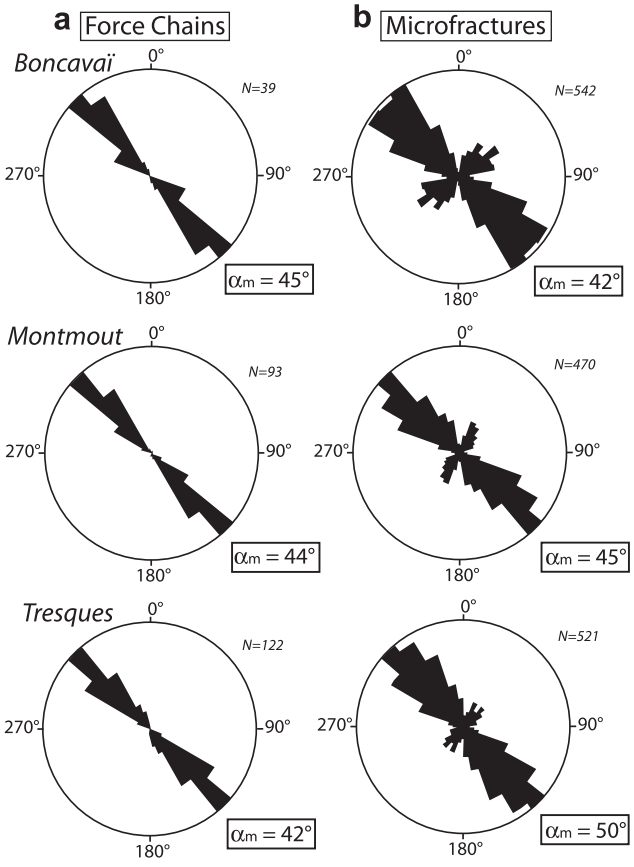

Fig. 11. Rose diagrams showing the trends of force chains (a) and grain microfractures (b).

The shear-enhanced compaction bands formed at quite shallow burial conditions. Given that the bands formed before the fold formation, which implies that Miocene and recent deposits should not be included in the burial depth estimation for the time of band formation, only the upper Cretaceous deposits above the Turonian sand-dominated unit (160 m of Turonian; 150 m of Santonian; 50 m of Coniacian) and potentially thin Paleocene-Eocene deposits should be included (Sornay, 1950; Ferry, 1997). This approach indicates that the SECBs form at about 400 m ± 100 m. As proposed by Soliva et al. (in press), shallow burial conditions coupled with coarse-grained porous sands and contractional tectonics promote the formation of shear-enhanced compaction bands (with a low ratio of shear to compaction) rather than the more common shear-dominated type of deformation bands.

6.2. Implications for sandstone reservoirs

Shear-enhanced compaction bands do not involve sufficient grain-scale deformation and related permeability reduction to control subsurface fluid flow. The bands consist of crush microbreccia characterized by a microclast proportion that amounts to less than 10%, a small grain-size reduction (Fig. 9), and a high microfracture density (Fig. 7, Fig. 8a and Fig. 10b). Grain shape is also generally preserved and the porous network shows only small reductions of porosity and pore throat size (Fig. 12a). These reductions are smaller than those commonly observed in cataclastic shear bands (Antonellini and Aydin, 1994; Tueckmantel et al., 2010). In general, the main porosity-reducing process in cataclastic bands is the infilling of pores by small grain fragments produced by grain comminution (Antonellini and Aydin, 1994;

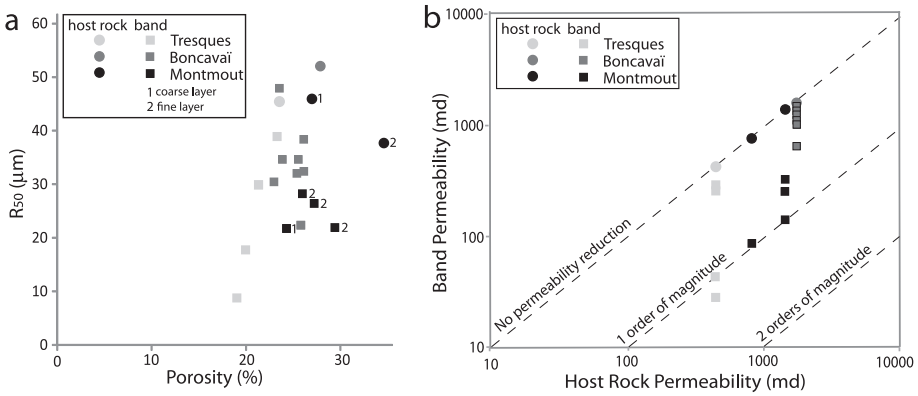

Fig. 12. a. Plot of the porosity vs median pore access radius (R_{50}). b. Permeability of deformation bands in relation to the surrounding host rock. Permeability has been calculated on band of centimeter scale using the Kozeny–Carman law.

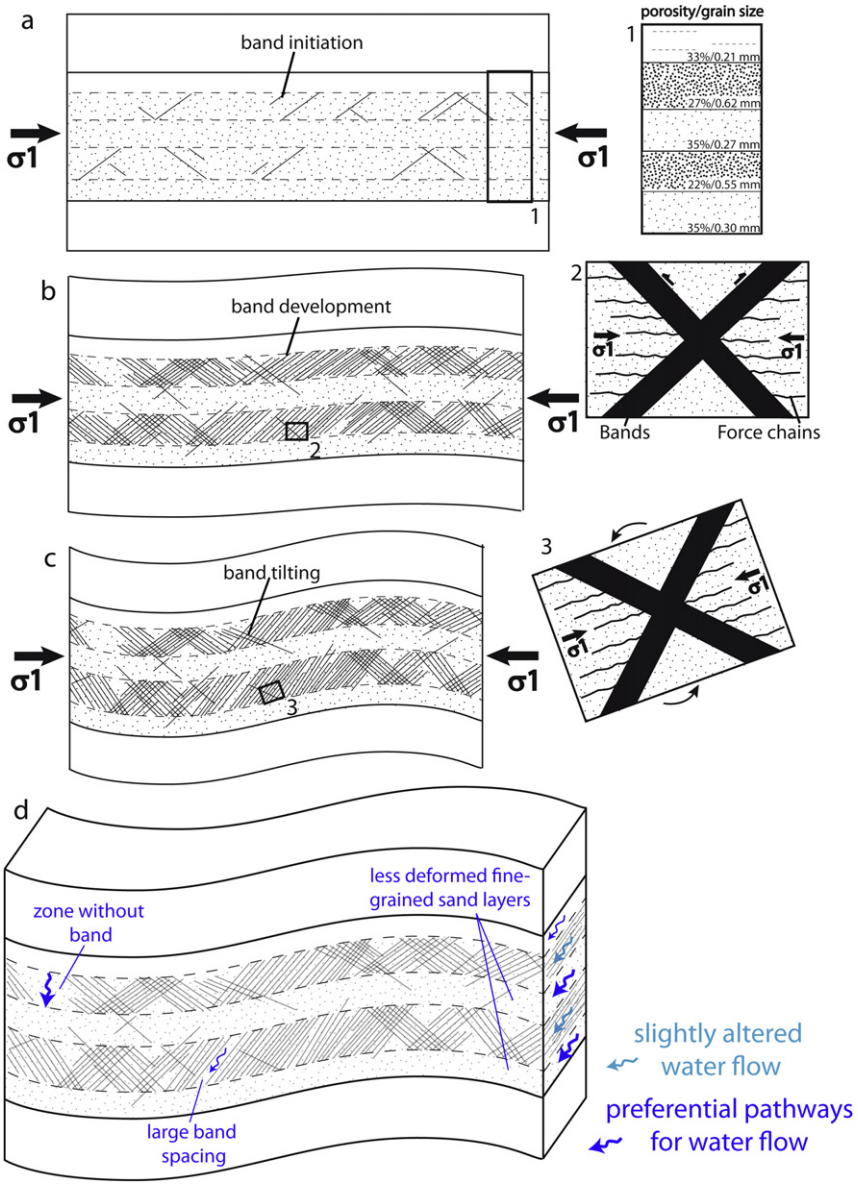

Fig. 13. Schematic illustration of the history of bands and folds. a. Initiation of SECBs at the beginning of the Pyrenean contraction, (1) shows the characteristics of the sand layers. b. Band development in coarse-grained sand layers at the initiation of fold formation, (2) shows the conjugate bands and the force chains. c. Tilting of bands in the fold limbs, (3) shows the tilting of bands and force chains at the microscale. d. Schematic diagram showing the relationship between the band network architecture and fluid flow in a reservoir setting. Note that layer thickness is exaggerated relative to the fold size.

David et al., 2001; Ballas et al., 2012) (excluding here any secondary cementation processes). In our case the presence of large pores implies that the microstructure of these SECBs is only slightly altered and suggests that large pore collapse has not occurred in these bands. The permeability reduction measured across the shear-enhanced compaction bands in Provence is rarely greater than 1 order of magnitude (Fig. 12b), and these bands show no influence on the localization of later alteration products (Fig. 6). These features suggest that the SECBs did not restrict the flow of the meteoric water responsible for the alteration. Hence, the patterns are not merely a result of fluids being able to flow within or along the bands. A complementary study focusing on the normal-sense shear bands in the Boncavaï quarry suggests a threshold of permeability reduction at around 2 orders of magnitude between bands limiting the alteration products and bands that do not (Ballas et al., 2012). Our SECBs involve too little cataclasis (crush microbreccia) to significantly modify the porous network of the sand, and are therefore too permeable to control the localization of the alteration products and to impact the flow of water under vadose and phreatic conditions.

The presence of Provence-type SECBs in a reservoir setting seems to represent limited concern for reservoir management. Sternlof et al. (2006) have, by flow simulation models, explored the impact of the compaction bands of Valley of Fire on fluid flow, finding a mild directional component to the pressure effect and pronounced tendency for fluid flow along the band trend. However, the 10–20% reduction of the reservoir transmissibility imposed by the SECBs of Provence seems too small to significantly affect fluid flow. This conclusion is corroborated by the flow simulations realized by Rotevatn et al. (2009) for deformation bands with permeability reduction less than 1 order of magnitude in a relay ramp. Small effects induced by the presence of Provence-type SECBs, such as an increase of flow tortuosity that involves band-parallel channeling of fluids and a delayed water breakthrough, cannot be totally excluded. However, a comprehensive flow simulation analysis would be needed to consider their field-specific effect during fluid injection or withdrawal for a reservoir containing such SECBs.

The specific occurrence of the shear-enhanced compaction bands in coarse-grained and less porous sandstone layers implies that the fine-grained and more permeable layers of the sandstone reservoir, unaffected by deformation bands, can constitute pathways for fluid flow (Fig. 13d). This observation supports the idea that grain size strongly influences band localization in sands, in agreement with field-based observations made by Antonellini et al. (1994), Mollema and Antonellini (1996), Schultz et al. (2010), and Fossen et al. (2011), and with mechanical testing results reported by Wong et al. (1997), Baud et al. (2004), and Fortin et al. (2005). Furthermore, the sand layers with high band density, i.e. with bands making up 17–22% of the cross-sectional surface of these layers, contain some up to several meters long parts that lack deformation bands or show unusually large band spacing. Clearly such intervals can constitute preferential pathways for fluid flow parallel to the strike of the bands within the sand layer with the greater band density (Fig. 13d).

6.3. Comparison with similar bands in the western US

Pure and shear-enhanced compaction bands have been described in Jurassic Navajo and Aztec Sandstones in the western United States, notably in the Buckskin Gulch area in southernmost Utah (Mollema and Antonellini, 1996; Schultz et al., 2010; Fossen et al., 2011) and in the Valley of Fire State Park in SE Nevada (Sternlof et al., 2005, 2006; Aydin and Ahmadov, 2009; Eichhubl et al., 2010). The shear-enhanced compaction bands of Valley of Fire localized bleaching due to meteoric water flow in oxidized rock in vadose conditions and therefore act as membrane seals in this context (e.g. Eichhubl et al., 2004) (Fig. 14a). In contrast, the SECBs in Provence did not localize or compartmentalize staining/bleaching patterns. It is therefore interesting to compare these two types of SECBs to understand why they differ in their influence of groundwater flow.

The SECBs in the Valley of Fire (VoF) show an organization that is quite similar to that observed in Provence, i.e. conjugate and distributed networks, no apparent shear offset and a similar range in thickness (Sternlof et al., 2004; Eichhubl et al., 2010). However, the VoF shear-enhanced compaction bands are less densely spaced (mean band spacing about 16 cm in VoF versus 2.5 cm in Provence), more sinuous, and more cohesive than the Provence ones (e.g., Sternlof et al., 2004) (Fig. 14a). Pressure solution at grain contacts and cataclastic deformation were inferred from the microstructure of VoF bands (Fig. 14b). Quartz cementation was also described by Eichhubl et al. (2010) and interpreted to be potentially synchronous with the band formation. Together, these inferences suggest that the burial depth estimated at the time of deformation (i.e. 0.54–1.1 km by Schultz (2009) and 0.75 km by Eichhubl et al. (2010)) were sufficient to activate quartz pressure-solution. In a common geothermal gradient, this range of depth would imply a temperature of ~30°, which could be considered as unexpected since this process has been documented to be significant only at temperatures in excess of 80–90° (Renard et al., 1997). A second interpretation would be to postulate post-deformation diagenesis at burial conditions of 2–3 km underneath the Cretaceous thrust sheet, an interpretation that would help to explain observations of preferred quartz overgrowth along grain fracture surfaces (e.g. Fisher and Knipe, 2001).

These solution-precipitation processes dramatically affect the porous network structure, imposing a significant decrease in the pore access radii and the connected porosity (Sun et al., 2011). Dissolution–cementation is therefore a process that created a reduction in permeability in the SECBs of Valley of Fire of more than 2 orders of magnitude based on the methodology explained in Section 5.1 (Fig. 14c). These values are consistent with the permeability measured by Fossen et al. (2011) on the SECBs from the Buckskin Gulch area. The Buckskin Gulch SECBs also show an abundance of structures related to grain-contact dissolution and the sandstone has experienced a maximum burial depth close to 2 km (Fossen et al., 2011). However, the permeability measurements that we determined for SECBs from VoF are more than 1 order of magnitude greater than those reported by Sun et al. (2011) from the same area (Fig. 14c). This difference could be due to (1) the different methods used for the permeability measurements, which were based on two-dimensional tomographic images and numerical method for Sun et al. (2011) versus the Kozeny–Carman law for this paper; and/or (2) local differences in the amount of deformation and cementation/solution in the sampled bands.

The dissolution–cementation process and the related 2 orders of magnitude permeability reduction identified in SECBs of Valley of Fire explain why they acted as membrane seals for meteoric water flow. In the SECBs of Provence, permeability reduction is rarely more than 1 order of magnitude (Fig. 12a). This permeability reduction is similar to the bed-parallel compaction bands described by Aydin and Ahmadov (2009) (Fig. 14c). The SECBs of Provence and the bed-parallel compaction bands from the VoF show no evidence of control on water flow. Altogether, this comparative analysis allows us to identify a threshold value of 2 orders of magnitude of permeability reduction for the SECBs above which they may significantly influence subsurface water flow (e.g. Ballas et al., 2012). This comparative analysis underscores the role of burial depth or specific P-T conditions at the time of band formation, and

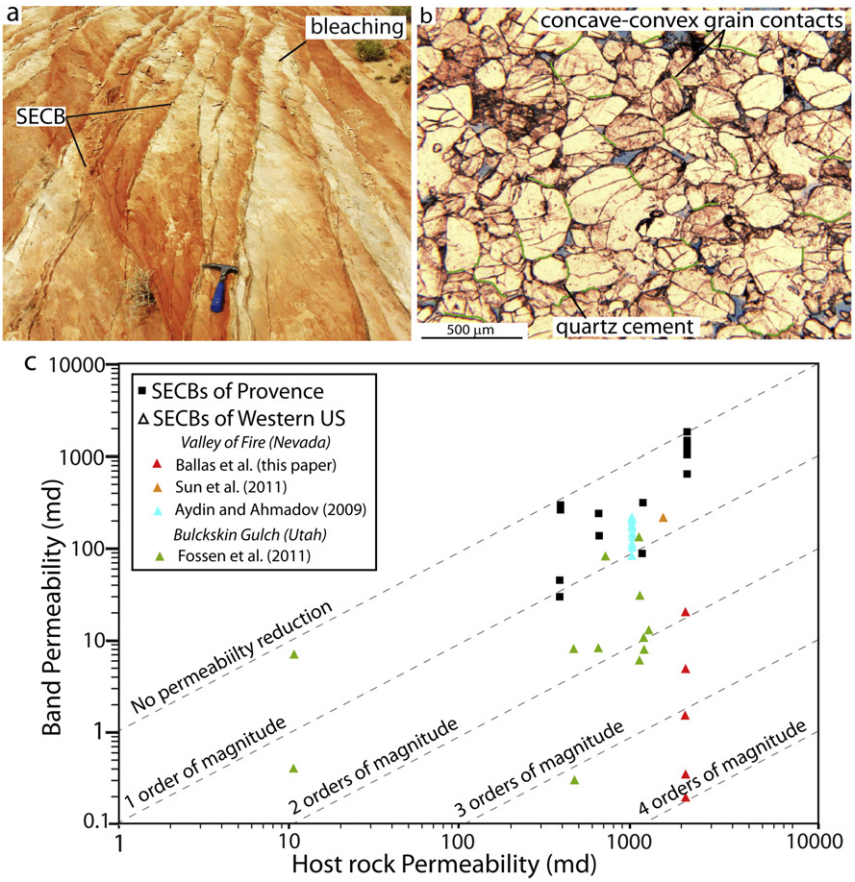

Fig. 14. a. Shear-enhanced compaction bands from the Valley of Fire (VoF) State Park. b. Photomicrograph of a SECB from VoF. c. Plot of band permeability vs. host rock permeability. The SECBs from the VoF State Park show greater reduction in permeability than those from the Buckskin Gulch area than Provence.

the effect of post-deformation diagenesis on the sealing properties of deformation bands.

7. Conclusions

This study shows that conjugate networks of shear-enhanced compaction bands formed at shallow burial conditions (400 m ± 100 m) during the Pyrenean contraction phase that also involved fold development. The bands are organized into conjugate and densely distributed networks preferentially located within the coarse-grained and less porous sand layers. Microtexturally, these bands classify as crush microbreccia as they are characterized by modest grain comminution and compaction, and a large microfracture density. The relatively low intensity of cataclastic deformation in these bands causes relatively small petrophysical property changes (3–8% reduction in porosity, 0–1 order of magnitude reduction in permeability) as compared to many other cataclastic shear band populations. These bands have no impact on the alteration products, which suggests that they impose no significant control on water flow under vadose and phreatic conditions. Hence, the microstructural deformation and the related petrophysical property variations induced by these SECBs are too small to significantly affect the reservoir transmissibility multiplier (10% and 20% reduction in transmissibility), and too confined to specific layers to compartmentalize the sandstone reservoir.

A comparison with similar bands in the US suggests that SECBs can be significant membrane seal barriers for deeper burial conditions (≥1 km), where pressure-solution and cementation processes trigger greater porosity and permeability reductions. This interpretation implicitly suggests that the burial depth, including the post-deformational burial history that can involve secondary cementation and dissolution, is a very important aspect to consider during the evaluation of the sealing potential of SECBs and deformation bands in general.

Acknowledgments

This work was supported by the Laboratory of Geosciences Montpellier and by AREVA NC, which are gratefully acknowledged. Additional support to Fossen and Skurtveit was provided through the IMPACT (429 207806/E20) and COPS projects funded by the Research Council of Norway and Statoil. We would like to thank Delorme, Veolia, and Sablex NC for giving us access to their quarries. We thank L. Zuluaga, and R.A. Schultz for their valuable assistance during the US filed trip. Doriane Delmas and Christophe Nevado are thanked for the preparation of the thin-sections. Thoughtful reviews by unknown reviewers together with helpful editorial comments from William Dunne improved the contents of this paper.

Appendix A. Supplementary data

Supplementary data related to this article can be found at http://dx.doi.org/10.1016/j.jsg.2012.11.008.

References

Antonellini, M.A., Aydin, A., 1994. Effect of faulting on fluid flow in sandstones, petrophysical properties. American Association of Petroleum Geologists Bulletin 78, 355–377.

Antonellini, M.A., Aydin, A., Pollard, D.D., 1994. Microstructures of deformation bands in porous sandstones at Arches National Park, Utah. Journal of Structural Geology 16, 941–959.
Antonellini, M.A., Aydin, A., 1995. Effect of faulting on fluid flow in sandstones, geometry and spatial distribution. American Association of Petroleum Geologists Bulletin 78, 642–671.
Arthaud, F., Matte, P., 1975. Les décrochements tardi-hercyniens du sud-ouest de l'Europe. Géométrie et essai de reconstitution des conditions de la déformation. Tectonophysics 25, 139–171.
Aydin, A., 1978. Small faults formed as deformation bands in sandstone. Pure and Applied Geophysics 116, 913–930.
Aydin, A., Borja, R.I., Eichhubl, P., 2006. Geological and mathematical framework for failure modes in granular rock. Journal of Structural Geology 28, 83–98.
Aydin, A., Ahmadov, R., 2009. Bed-parallel compaction bands in aeolian sandstone: their identification, characterization and implications. Tectonophysics 479, 277–284.
Ballas, G., Soliva, R., Sizun, J.-P., Benedicto, A., Cavailhes, T., Raynaud, S., 2012. The importance of the degree of cataclasis in shear bands for fluid flow in porous sandstone (Provence, FRANCE). American Association of Petroleum Geologists Bulletin 96, 2167–2186.
Baud, P., Klein, E., Wong, T.-F., 2004. Compaction localization in porous sandstones: spatial evolution of damage and acoustic emission activity. Journal of Structural Geology 26, 603–624.
David, C., Menendez, B., Zhu, W., Wong, T.-F., 2001. Mechanical compaction, microstructures and permeability evolution in sands. Physics and Chemistry of the Earth (A) 26, 45–51.
Debrand-Passard, S., Courbouleix, S., Lienhardt, M.J., 1984. Synthèse géologique du Sud – Est de la France: Stratigraphie et paléogéographie. Bureau de Recherches Géologiques et Minières. Mémoire 215, Orléans.
Du Bernard, X., Eichhubl, P., Aydin, A., 2002. Dilation bands: a new form of localized failure in granular media. Geophysical Research Letters 29 (24), 2176.
Eichhubl, P., Taylor, W.L., Pollard, D.D., Aydin, A., 2004. Paleofluid flow and deformation in the Aztec sandstone, at the Valley of Fire, Nevada – evidence for the coupling hydrogeological, diagenetic and tectonic processes. Geological Society of American Bulletin 116, 1120–1136.
Eichhubl, P., Hooker, J., Laubach, S.E., 2010. Pure and shear-enhanced compaction bands in Aztec Sandstone. Journal of Structural Geology 32, 1873–1886.
Ferry, S., 1997. Apport des forages ANDRA de Marcoule à la connaissance de la marge crétacée rhodanienne. In: Etude du Gard Rhodanien (Ed.), Actes des Journées Scientifiques CNRS/ANDRA. EDP sciences, Bagnols-sur-Cèze, pp. 63–91.
Fisher, Q.J., Knipe, R.J., 2001. The permeability of faults within siliciclastic petroleum reservoirs of the North Sea and Norwegian Continental Shelf. Marine and Petroleum Geology 18, 1063–1081.
Fortin, J., Schubnel, A., Guégen, Y., 2005. Elastic wave velocities and permeability evolution during compaction of Bleurswiller sandstone. International Journal of Rock Mechanics & Mining Sciences 42, 873–889.
Fossen, H., Schultz, R.A., Shipton, Z.K., Mair, K., 2007. Deformation bands in sandstone: a review. Journal of the Geological Society, London 164, 755–769.
Fossen, H., Bale, A., 2007. Deformation bands and their influence on fluid flow. American Association of Petroleum Geologists Bulletin 91, 1685–1700.
Fossen, H., Schultz, R.A., Torabi, A., 2011. Conditions and implications for compaction band formation in the Navajo Sandstone, Utah. Journal of Structural Geology 33, 1477–1490.
Lacombe, O., Jolivet, L., 2005. Structural and kinematic relationships between Corsica and the Pyrenees-Provence domain at the time of the Pyrenean orogeny. Tectonics 24, 1–20.
Manzocchi, T., Walsh, J.J., Nell, P., Yielding, G., 1999. Fault transmissibility multipliers for flow simulation models. Petroleum Geoscience 5, 53–63.
Mollema, P.N., Antonellini, M.A., 1996. Compaction bands: a structural analog for anti-mode I cracks in aeolian sandstone. Tectonophysics 267, 209–228.
Ogilvie, S.R., Glover, P.W.J., 2001. The petrophysical properties of deformation bands in relation to their microstructure. Earth and Planetary Science Letters 193, 129–142.
Olsson, W.A., 2000. Origin of Lüders' bands in deformed rock. Journal of Geophysical Research 105, 5931–5938.
Parry, W.T., Chan, M.A., Beitler, B., 2004. Chemical bleaching indicates episodes of fluid flow in deformation bands in sandstone. American Association of Petroleum Geologists Bulletin 88, 175–191.
Potter, S.L., Chan, M.A., 2011. Joint controlled fluid flow patterns and iron mass transfer in Jurassic Navajo Sandstone, Southern Utah, USA. Geofluids 11, 184–198.
Renard, F., Ortoleva, P., Gratier, J.-P., 1997. Pressure solution in sandstones: Influence of clays and dependence on temperature and stress. Tectonophysics 280, 257–266.
Rotevatn, A., Tveranger, J., Howell, J.A., Fossen, H., 2009. Dynamic investigation of the effect of a relay ramp on simulated fluid flow: geocellular modeling of the Delicate Arch Ramp, Utah. Petroleum Geoscience 15, 45–58.
Saillet, E., 2009. La localisation de la déformation dans les grés poreux: caractérisation d'un analogue de réservoir gréseux et faillé dans le Bassin du Sud-Est, Provence, France. Ph.D. thesis. University of Nice-Sophia Antipolis.
Saillet, E., Wibberley, C.A.J., 2010. Evolution of cataclastic faulting in high-porosity sandstone, Bassin du Sud-Est, Provence, France. Journal of Structural Geology 32, 1590–1608.
Sanchis, E., Seranne, M., 2000. Structural style and tectonic evolution of a polyphase extensional basin of the Gulf of Lion passive margin: the Tertiary Alès basin, southern France. Tectonophysics 322, 219–242.
Scholz, C.A., 1990. Mechanics of Earthquake and Faulting. Cambridge University Press.
Schultz, R.A., Siddharthan, R., 2005. A general framework for the occurrence and faulting of deformation bands in porous granular rocks. Tectonophysics 411, 1–18.
Schultz, R.A., Soliva, R., Fossen, H., Okubo, C.H., Reeves, D.M., 2008. Dependence of displacement-length scaling relations for fractures and deformation bands on the volumetric changes across them. Journal of Structural Geology 30, 1405–1411.
Schultz, R.A., 2009. Scaling and paleodepth of compaction bands, Nevada and Utah. Journal of Geophysical Research 114, 13.
Schultz, R.A., Okubo, C.H., Fossen, H., 2010. Porosity and grain size controls on compaction band formation in Jurassic Navajo Sandstone. Geophysical Research Letters 37, L22306. http://dx.doi.org/10.1029/2010GL044909.
Sibson, R.H., 1977. Fault rocks and fault mechanisms. Journal of the Geological Society 133, 191–213.
Soliva, R., Schultz, R.A., Ballas, G., Taboada, A., Wibberley, C.A.J., Saillet, E., Benedicto, A., in press. A model of strain localization in porous sandstone as a function of tectonic setting, burial and material properties; new insight from Provence (SE France). Journal of Structural Geology.
Sornay, J., 1950. Etude stratigraphique sur le Crétacé supérieur de la vallée du Rhône entre Valence et Avignon et des régions voisines. Ph.D. thesis. University of Grenoble.
Sternlof, K., Chapin, J.R., Pollard, D.D., Durlofsky, L.J., 2004. Effective permeability in sandstone containing deformation band arrays. American Association of Petroleum Geologists Bulletin 88, 1315–1329.
Sternlof, K., Rudnicki, J.W., Pollard, D.D., 2005. Anticrack inclusion model for compaction bands in sandstone. Journal of Geophysical Research 110, B11403.
Sternlof, K., Karimi-Fard, M., Pollard, D.D., Durlofsky, L.J., 2006. Flow and transport effects of compaction bands in sandstone at scales relevant to aquifer and reservoir management. Water Resources Research 42, W07425.
Sun, W., Andrade, J.E., Rudnicki, J.W., Eichhubl, P., 2011. Connecting microstructural attributes and permeability from 3D tomographic images of in situ shear-enhanced compaction bands using multiscale computations. Geophysical Research Letters 38, L10302.
Taylor, W.L., Pollard, D.D., 2000. Estimation of in situ permeability of deformation bands in porous sandstone, Valley of Fire, Nevada. Water Resources Research 36, 2595–2606.
Torabi, A., Fossen, H., Alaei, B., 2008. Application of spatial correlation functions in permeability estimation of deformation bands in porous rocks. Journal of Geophysical Research 113, B08208.
Tueckmantel, C., Fisher, Q.J., Knipe, R.J., Lickorish, H., Khalil, S.M., 2010. Fault seal prediction of seismic-scale normal faults in porous sandstone: a case study from the eastern Gulf of Suez rift, Egypt. Marine and Petroleum Geology 27, 334–350.
Wibberley, C.A.J., Petit, J.-P., Rives, T., 2007. The mechanics of fault distribution and localization in high-porosity sands, Provence, France. In: Lewis, H., Couples, G.D. (Eds.), The Relationship between Damage and Localization. Geological Society, London, Special Publications, vol. 164, pp. 599–608.
Wong, T.-f., David, C., Zhu, W., 1997. The transition from brittle faulting to cataclastic flow in porous sandstones: mechanical deformation. Journal of Geophysical Research 102, 3009–3025.